Design of Ni-based Bulk Metallic Glasses with Improved Mechanical and Corrosion Properties

Gayatri Tanuja Guddla[1], Suman Gandi[2], Satyadevi Ambadipudi[1] and Balaji Rao Ravuri[2]*

[1]Department of Mechanical Engineering, School of Technology, GITAM (Deemed to be University), Hyderabad, India
[2]Department of Physics, School of Science, GITAM (Deemed to be University), Hyderabad, India

Received: 30 January 2020, Revised: 11 August 2020, Accepted: 20 August 2020

Abstract

Bulk metallic glasses (BMGs) are synthesized using high energy mechanical ball milling technique with the general formula, $[Ni\text{-}Cr\text{-}Si]_{100-x}:Nb_x$ (x = 0, 3, 6 and 9 at.%, labelled as $NCSNb_0$, $NCSNb_3$, $NCSNb_6$, $NCSNb_9$). Interestingly, all the thermal, mechanical and corrosion properties are greatly enhanced with increase in Niobium (Nb) content up to 6 at.% ($NCSNb_6$). XRD analysis shows that the phase attribution over all the BMGs is due to Nickel (Ni, 98-006-0833), Chromium (Cr, 98-002-1500), Silicon (Si, 98-001-2990) and Niobium (Nb, 98-002-3331). The values of the largest super-cooled liquid region width and plastic strain attained are 232 K and 0.94±0.1%, for the $NCSNb_6$ BMG sample. The considerable addition of Niobium (Nb ~ 6 at.%) content in [Ni-Cr-Si] BMG network ($NCSNb_6$) is anticipated to have the best glass-forming ability, mechanical and corrosive resistant properties and is expected to be used as potential material for lightweight vehicle applications.

Keywords: glass-forming ability; bulk metallic glass; super-cooled liquid region
DOI……..

1. Introduction

Initially, the research area of amorphous glasses was focused on the scientific curiosity of how deeply nucleation and crystal growth could be arrested by under cooling liquids below their glass transition temperature, until 1960 when the metallic glass system, AuSi was first introduced [1]. After two decades of further research, the development of multi-component compositions with large atomic size mismatches between constituent elements with deep eutectics was proposed [2]. The discovery of bulk metallic glasses (BMGs) instigated a widespread research interest owing to their technological and scientific importance towards glass formation phenomena. Among the extensive family of glasses, BMGs are possibly the youngest, owing to a number of special characteristics like amorphocity, high strength, etc [3]. BMGs have attracted great attention, owing to their unique properties attained due to different atomic configuration. In recent investigations, significant advances in enhancing glass-forming abilities (GFA) have paved the way for their

*Corresponding author: Tel.: (+91) 08455221307
E-mail: balajirao.ravuri@gitam.edu

potential applications as functional and structural materials [4-8]. Perker and Johnson reported on the excellent glass-forming ability of the bulk metallic glass: $Zr_{41.2}Ti_{13.8}Cu_{12.5}Ni_{10.0}Be_{22.5}$, prepared by the metal casting method [9]. As per Park and Kim, by successfully designing the BMG matrix, the plasticity can be controlled effectively [10].

Feng *et al*. designed a new matrix by proportional mixing of binary alloys $Cu_{50}Zr_{50}$ and $Cu_{73}Ti_{27}$ and investigated their thermal, mechanical and corrosion properties including glass-forming abilities [11]. Similarly, Wang and Li investigated bulk metallic glass formation in the binary Cu-Zr system, prepared by the copper mould casting system [12]. Furthermore, Xia *et al*. [13] reported $Ni_{62}Nb_{38}$ as the best glass former composition upon investigating binary Ni-Nb bulk metallic glasses. Several studies reported the glass-forming abilities and thermal stability of ternary Ca-Mg-Zn BMG [14, 15]. Sun *et al*. [16] introduced Zr-Cu-Ni-Al quaternary amorphous alloy compositions with super high glass-forming ability. Liu and Lu [17] provided a comprehensive review of the effect of minor doping on the glass-forming properties in BMGs and stated that the glass-forming ability was enhanced considerably using small amounts (usually < 2 at. %) of B, Si, Y and Sc.

Kui *et al*. [18] found that there was no crystallinity found in the glass alloy $Pd_{40}Ni_{40}P_{20}$ that had been consistently undercooled, via X-ray diffraction, SEM studies and calorimetry. Several researchers studied the microstructure and corrosion behavior of extruded Mg-4Zn-2Gd-0.5Ca Alloy [19-24]. Many studies have proposed a parameter γ to quantify the glass-forming ability of BMGs. They have also discussed the limitations of all the discussed GFA parameters [25-28]. Many research findings reported the improvements in the mechanical and corrosion properties of Ni-Mo coatings through the incorporation of Y_2O_3 nanoparticles [29-36]. Trexler and Thadhani [37] studied the mechanical properties of bulk metallic glasses in detail, including their superior strength, hardness, excellent wear and corrosion resistance. Wang *et al.* [38] reported the effects of Cr contents in Fe-based bulk metallic glasses $Fe_{69.9-x}C_{7.1}Si_{3.3}B_{5.5}P_{8.7}Cr_xMo_{2.5}Al_{2.0}Co_{1.0}$ (x = 0.0, 2.3-12.3) (fabricated using industrial raw materials) on the glass-forming ability and corrosion resistance. They found that the GFA decreases and corrosion resistance increases with the addition of Cr content.

Chang *et al*. [39] studied the microstructure and mechanical properties of Ni-Cr-Si-B-Fe composite coating that had been fabricated by laser additive manufacturing and found that this composite exhibited excellent wear resistance. Qiu *et al*. [40] concluded that addition of small amounts of Niobium, Nb (0, 2, 5 at.%) enhances the strength and plasticity of the base alloy $Zr_{65-x}Nb_xCu_{17.5}Ni_{10}Al_{7.5}$ as a result of the rapid formation of a highly protective passive film.

Inspired by all these results, we have examined the glass-forming abilities, thermal properties, mechanical and corrosion properties of the ternary BMG matrix [Ni-Cr-Si], which was doped with Niobium at various concentrations, Nb_x (x = 0, 3, 6 and 9 at.%) and characterized by XRD, DTA, Vicker's hardness test, Uniaxial compression test, Polarization test and then SEM before and after corrosion test. It is understood that minor alloying can greatly affect the performance of BMGs. Doping with Niobium (Nb) offers excellent resistance to oxidation and corrosion and even 0.1% Niobium (Nb) can significantly enhance the performance characteristics of metals.

2. Materials and Methods

The base metal matrix [Ni-Cr-Si] was prepared with pure metal powders of high purity: Nickel (Ni, 99.99 Wt.%), Chromium (Cr, 99.99 Wt.%) and Silicon (Si, 99.99 Wt.%), each with 33.33 At. Wt.%, which were mixed well in an agate mortar, for a period of 30 min to form a homogenous mixture. This base metallic powder (BMG) was doped with Niobium (Nb, 99.99 Wt.%) using the general formula, $[Ni\text{-}Cr\text{-}Si]_{100-x}$:$[Nb]_x$, (x = 0, 3, 6 and 9 at.% and labelled as $NCSNb_0$, $NCSNb_3$,

$NCSNb_6$ and $NCSNb_9$). Further synthesis of this metal composition was carried out using a high energy mechanical ball milling apparatus in which it was further mixed and crushed to micro size, using a tungsten crucible, with powder to balls ratio taken as 1:10 with a rotation speed of 300 rpm, for about 30 h. The tungsten carbide vials were initially evacuated and purged under pressure of $3x10^5$ Pa. In order to control the agglomeration of the particles, the entire milling process was carried out in a wet medium using 30 ml hexane. At the end of successful ball milling, the samples were dried for about 5 h using a vacuum oven (i-therm, AI-7981Model) at 350 K and collected in powdered form and then analyzed with the help of ICP Spectroscopy. The amorphous nature of the sample and phase analysis was studied via XRD analysis and this was carried out using an Empyrean PANalytical X-rays diffractometer instrument using Co-Kα radiation with a step size of 0.02o with 60 kV tube voltage and 5 mA of tube current for a period of 20 s/step, prior to and post ball milling. A Jeol JEM-1010 electron microscope was used to obtain TEM-scanned images to analyze the surface morphologies. In order to be sure that the samples to be tested were electrically conductive and dry, some sample preparation was done by embedding the BMG powder sample in a copper foil at first, using electrodeposition for mechanical thinning. For electron transparency, ion milling was used and a high energy electron beam was focused on the sample to achieve highly magnified and complex images to better understand the topography of the sample.

The thermal properties were characterized using a Thermo-Gravity/ Differential Thermal Analysis (TG/DTA) analysis (CMET, Pan: Alumina). It was carried out with nitrogen gas at a heating rate of 40 K/min for 0.5s and 10 cel./min and a temperature range of 300 K-1300 K. Through this process, sharp endothermic peaks indicated any phase changes such as melting or fusion, and broad exothermic peaks revealed any dehydration reactions or chemical reactions including oxidation [41]. Then the BMG samples were put n into a vacuum hot-pressing machine and the pressing was carried out with a pressure of 1.2 GPa at its T_c for about an hour, to obtain green pellets of 10mm X 2mm size.

Vickers indenter (Wolpert Wilson, Universal 930/250 N DigiTestor) was used to measure the microhardness of the samples under a load of 1 kg with a dwell time of 10s. A 3369 Uniaxial Compression testing machine was used to perform compression tests with a loading rate of 2X10-4/s and an aspect ratio of 2:1. The corrosive nature of the prepared samples was investigated using an electrochemical polarization technique with RST500F device in 0.5 M HCL aqueous solution from -2.5V-5.5V at a potential sweep rate of 0.05mV/s. This test was done with a standard SCE (Saturated Calomel Electrode) as a reference electrode. The counter electrode was a three-electrode cell, with a platinum foil. The samples were exposed to open air for about 20 min prior to the electrochemical measurements set up, to stabilize the open-circuit potentials [42]. SEM, JEOL, and JSM-6700F instruments were used to study the structural morphologies and find the crystallite sizes of the samples at 20kV, prior to and post corrosion test.

3. Results and Discussion

From XRD studies, we obtained the crystallite sizes, lattice strains and phase identifications of the BMG powder mixtures before and after ball milling for 30 h, using X'pert high score plus software. The energy utilized throughout the milling process depends on the degree of crystalline and amorphous phases present in the BMG matrix. The XRD profiles of all synthesized BMG samples ($NCSNb_0$, $NCSNb_3$, $NCSNb_6$, and $NCSNb_9$), prior to the ball milling process, are displayed in Figure 1. The peak positions of the diffraction peaks, aroused due to Nickel (Ni, 98-006-0833), Chromium (Cr, 98-002-1500), Silicon (Si, 98-001-2990) and Niobium (Nb, 98-002-3331) crystalline phases, at 0 h of ball milling are shown in Figure 1.

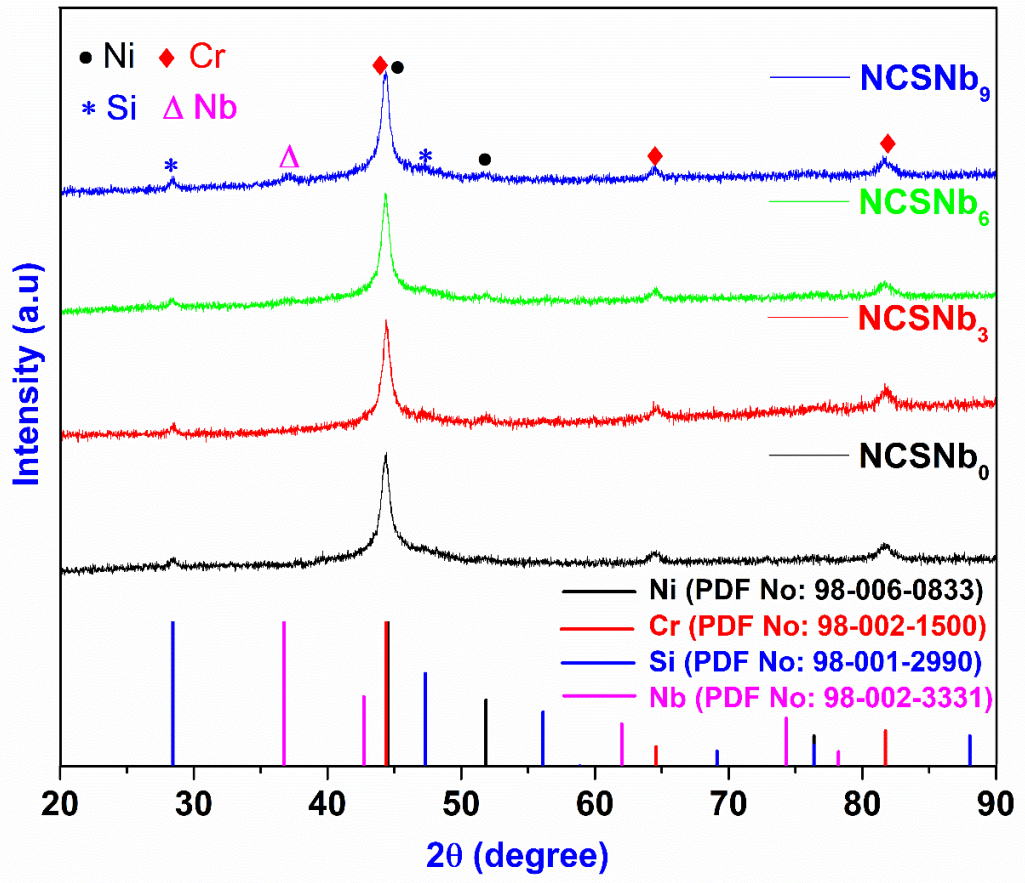

Figure 1. XRD profile of all $NCSNb_x$ BMG samples ($NCSNb_0$, $NCSNb_3$, $NCSNb_6$ and $NCSNb_9$) before ball milling

Upon subsequent prolonged hours of milling, from 0 to 30 h most of the crystalline peak intensities start decreasing and almost disappeared at 30 h milling time. However, few broad peaks that conform to a typical amorphous state are retained (Figure 2). Hence, it is expected that 30 h milling time is adequate to obtain the amorphization phase of the $NCSNb_x$ BMG samples. Furthermore, the broad peaks of the sample containing 6 at.% of Nb content ($NCSNb_6$), slightly shift to a lower position compared to the other prepared BMG samples ($NCSNb_0$, $NCSNb_3$, and $NCSNb_9$) owing to the degree of amorphous nature that develops due to the nucleation process of Nb content [43]. This tendency reveals that the $NCSNb_6$ BMG sample comprises more than 95% of the original compound and is expected to possess the best glass-forming ability (GFA).

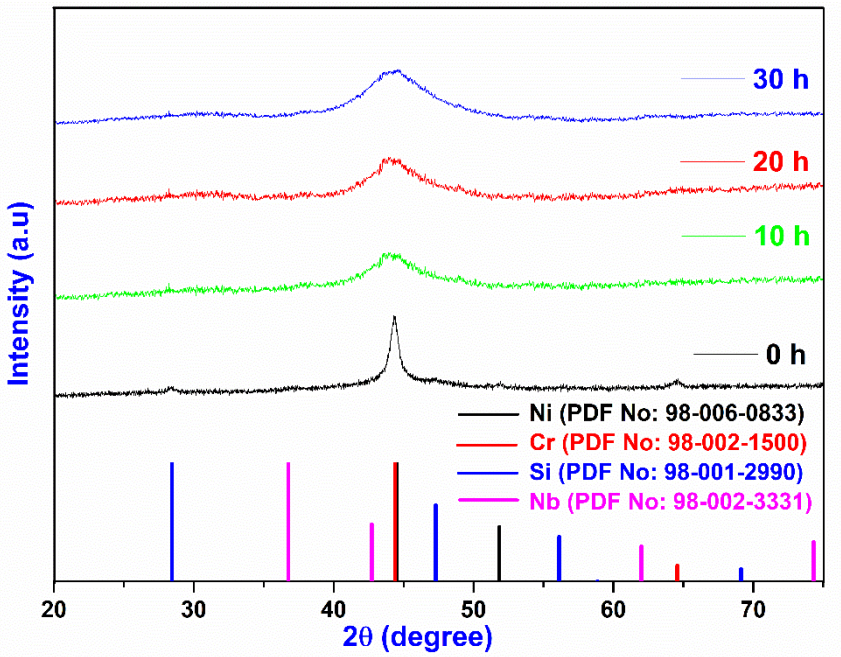

Figure 2. XRD peak patterns of the composition $[Ni\text{-}Mo\text{-}Si]_{94}$:$[Nb]_6$ ($NCSNb_6$ BMG Matrix), as a function of milling time

To further justify the amorphous nature of the $NCSNb_6$ BMG sample, the TEM bright-field image at 30 h milling time is displayed in Figure 3. An interesting blend of the crystalline phase, which is precipitated together with an amorphous phase is seen in Figure 3. This can be attributed to the active participation of Niobium (Nb) nano-crystallites in the nucleation process so as to promote the rate of crystallization during the hot-pressing process. The overall XRD analysis can be summarized as follows: i) All prepared BMG samples, $NCSNb_0$, $NCSNb_3$ and $NCSNb_9$ have shown considerable crystalline peaks that are higher than $NCSNb_6$ sample, ii) Also, $NCSNb_0$, $NCSNb_3$ and $NCSNb_9$ BMG samples exhibited poor amorphization tendencies when compared to $NCSNb_6$ sample. This shows that the BMG sample containing Niobium (Nb) composition of 6 at.% ($NCSNb_6$) exhibits superior glass-forming abilities and a decrease in surface roughness because of the incorporation of Niobium (Nb) into the Ni-Mo-Si matrix. This is attributed to the aggregation of Niobium (Nb) nano-crystallites which are expected to create an impact on improved corrosion resistance properties [44]. As such, more emphasis is laid on the structural properties, mechanical and corrosion behavior of $NCSNb_6$ BMG sample in coming up sections. Using the Scherer formula, the average sizes of the crystallites were found to vary from 41 nm to 60 nm as a function of Niobium (Nb) content (Table 1).

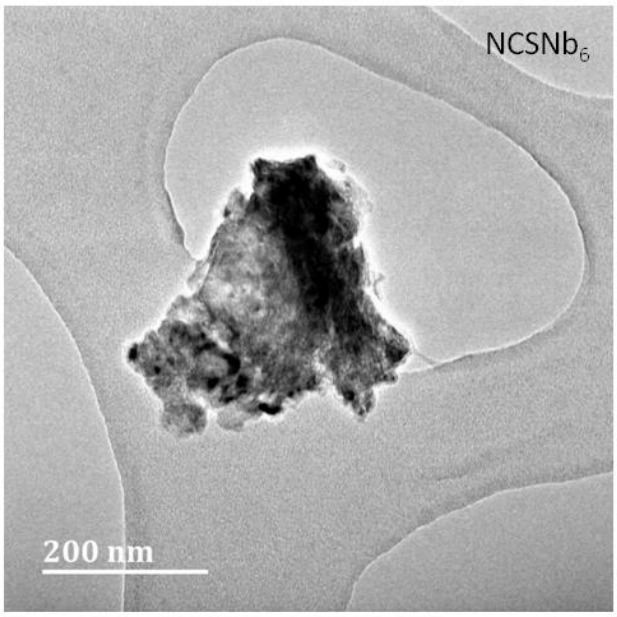

Figure 3. TEM bright-field image of $NCSNb_6$ BMG sample

Table 1. Crystallite size and lattice strain of all as-prepared $NCSNb_x$ BMG samples at 30 h of ball milling

BMG	Crystallite size (nm)	Lattice strain (%)
$NCSNb_0$	60	1.5
$NCSNb_3$	49	0.9
$NCSNb_6$	**41**	**0.4**
$NCSNb_9$	47	1.1

Based on the XRD analysis, the thermal stability and the glass-forming ability of all prepared $NCSNb_x$ BMG samples were measured at 30 h of ball milling and examined via DTA studies at a heating rate of 10 K/min and the results are shown in Figure 4. The endothermic profile of the DTA images is a primary characteristic that shows a glass transition phase, followed by a super-cooled liquid region and an exothermic crystalline reaction. As an example, for the Niobium free ($NCSNb_0$) sample, the glass transition temperature (T_g) is 627 K, and the crystallization temperature (T_c) is 764 K. Similarly, the super-cooled liquid region (ΔT) and liquidus temperature (T_l) are recorded to be 121 K and 1127 K respectively. Based on these studies, the thermal properties (T_g, T_c, T_l, $\Delta T=T_c-T_g$) and the parameter, γ ($=T_c/(T_g+T_l)$)) for all the as-prepared BMG samples are calculated after 30 h of ball milling and are tabulated in Table 2. From Table 2, the decreasing trend of ΔT values are found to be $NCSNb_6 > NCSNb_9 > NCSNb_3 > NCSNb_0$, which implies that $NCSNb_6$ sample possesses the best glass-forming characteristics when compared to all other BMG samples

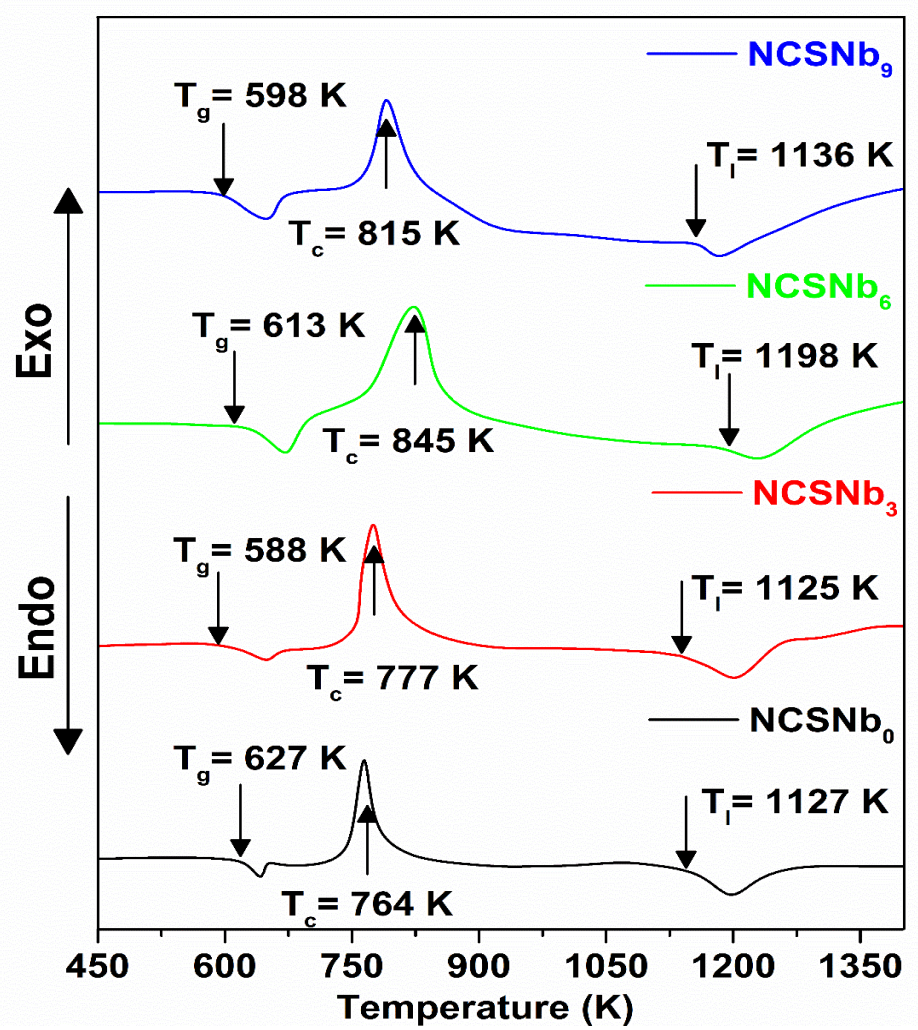

Figure 4. DTA profiles of all as-prepared $NCSNb_x$ BMG samples at 30 h of ball milling

Table 2. DTA parameters of all as-prepared $NCSNb_x$ BMG samples at 30 h of ball milling

BMG	T_g (K)	T_c (K)	T_l (K)	$\Delta T = T_c - T_g$ (K)	$\gamma = T_c/(T_g+T_l)$
$NCSNb_0$	627	764	1127	137	0.435
$NCSNb_3$	588	777	1125	189	0.453
$NCSNb_6$	**613**	**845**	**1198**	**232**	**0.466**
$NCSNb_9$	598	815	1136	217	0.470

under investigation. A higher ΔT represents higher thermal stability. As indicated in Figure 5 and Table 2, the addition of Nb strongly affects the thermal stability of BMGs. The value of ΔT increases from 137 K to a maximum value of 232 K with increasing Niobium content from 0 to 6

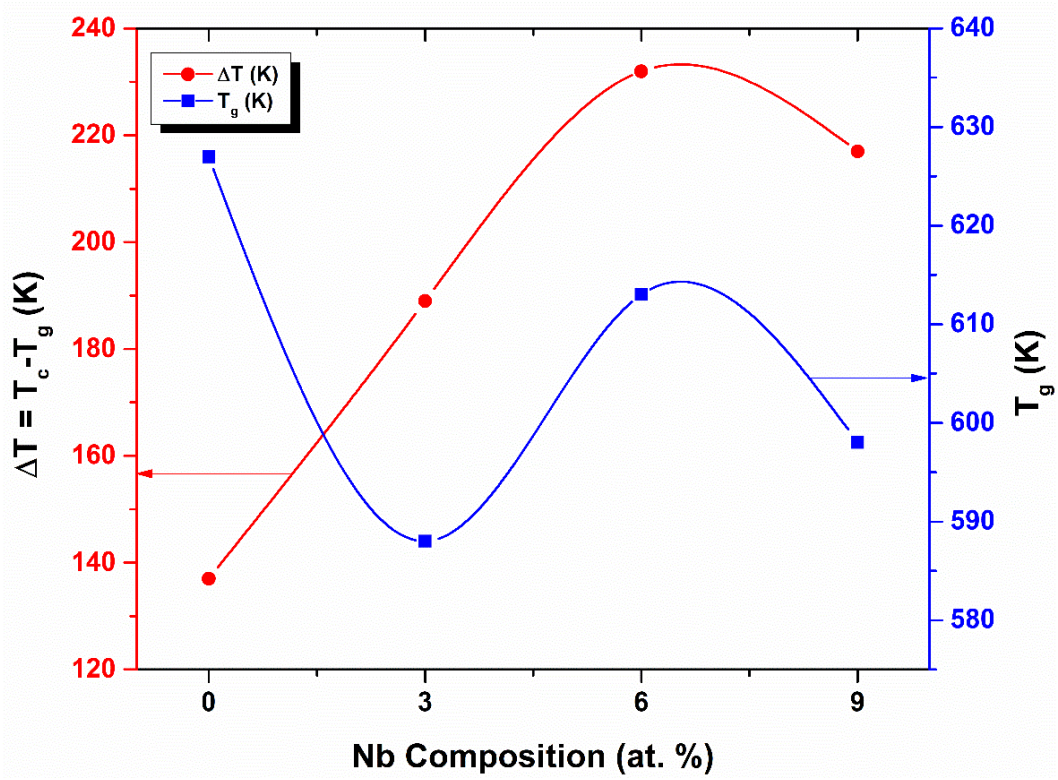

Figure 5. Variations of ΔT and T_g with Nb content of all as-prepared $NCSNb_x$ BMG samples

at.%, then decreases with increasing Niobium content from 6 at.% to 9 at.%. It is well known that γ and ΔT are important parameters for estimating glass-forming ability, and therefore higher γ and ΔT corresponds to higher glass forming ability [45].

The correlation behavior of T_g Vs ΔT with the Niobium (Nb) composition (at.%) is shown in Figure 5. The super-cooled liquid region, ΔT and γ are found to be highest for the sample having 6 at.% of Niobium ($NCSNb_6$). These results are in good agreement with the XRD studies. Additionally, the correlation between Vickers hardness values and plastic strain with respect to Niobium (Nb) composition is depicted in Figure 6. It is noteworthy that the sample with the best glass-forming ability ($NCSNb_6$) displayed the highest plastic strain and hardness, which is a significant contribution of this present family of BMG network (Figure 6 and Table 2). This could be due to the large negative heating effect generated with substantial doping of Niobium (Nb) content with base BMG matrix, [Ni-Cr-Si]. The other mechanical properties of all the as-prepared $NCSNb_x$ BMG samples were studied with the help of compressive stress-strain curves, and the results are shown in Figure 7. All the BMG samples exhibit a unique behavior of increasing stress with the increase of strain, which is in accordance with the law of elasticity and is also referred as work hardening. All the curves undergo an elastic deformation followed by a serrated plastic deformation before fracture failure occurs. The yield strength (σ_y), fracture strength (σ_f) and ε_p for all $NCSNb_x$ BMG samples are calculated from the stress-strain curves and are listed in Table 3. Nevertheless, the values of σ_y, σ_f and ε_p for the Niobium free ($NCSNb_0$) BMG sample are found to be 1701±27, 1732±12 and 0.33±0.1% respectively.

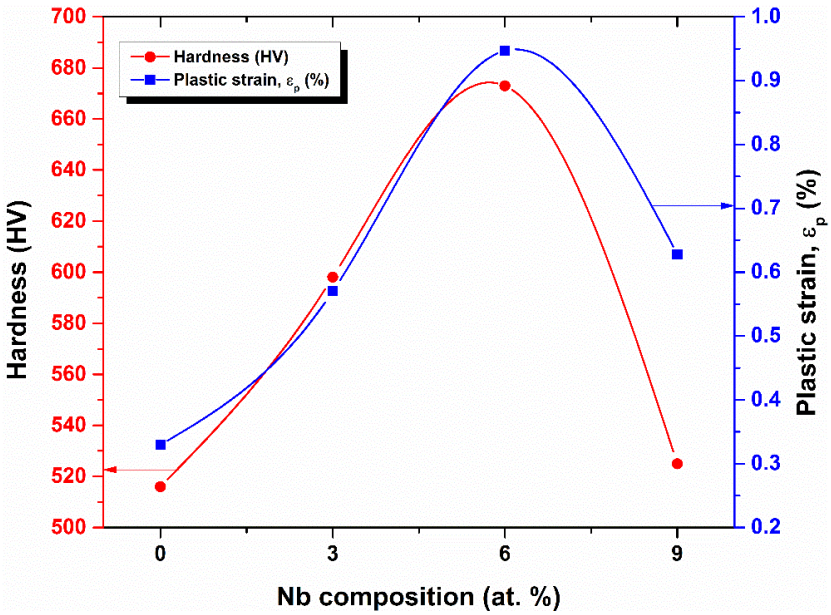

Figure 6. Correlation between Vickers hardness and plastic strain values of all prepared $NCSNb_x$ BMG samples

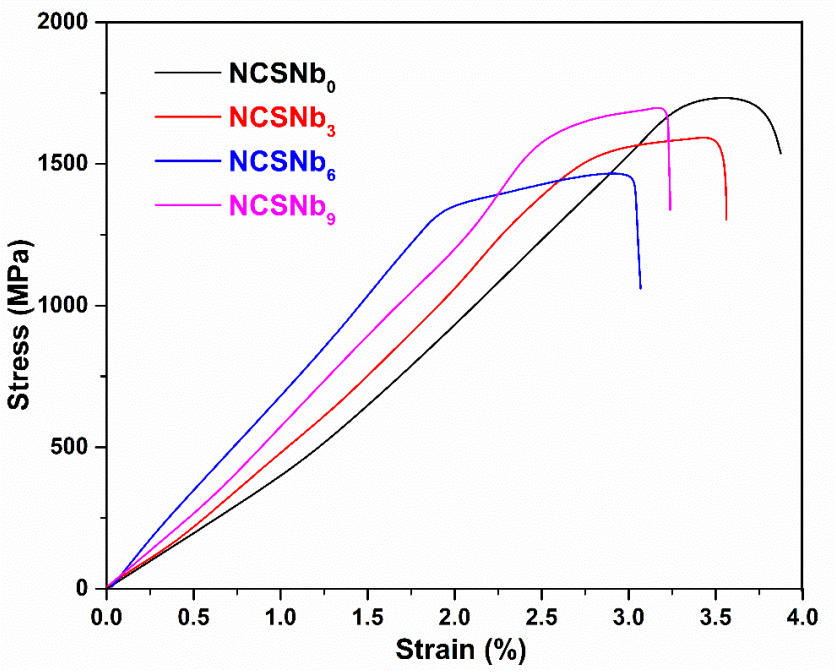

Figure 7. Engineering Stress-Strain curves of all $NCSNb_x$ BMG samples at 30 h of ball milling

Table 3. Yield strength (σ_y), fracture strength (σ_f), plastic strain (ε_p), and hardness values of all as-prepared $NCSNb_x$ BMG samples

BMG	σ_y (MPa)	σ_f (MPa)	ε_p (%)	Hardness (HV)
$NCSNb_0$	1701±27	1732±12	0.33±0.1	516
$NCSNb_3$	1549±35	1595±22	0.57±0.1	598
$NCSNb_6$	**1363±43**	**1467±45**	**0.947±0.1**	**673**
$NCSNb_9$	1605±23	1699±15	0.628±0.1	525

Figure 8 displays the compressive plasticity of all the as-prepared $NCSNb_x$ BMG samples and it is observed from Table 3 and Figure 8 that among all the prepared samples, the ε_p is maximum for $NCSNb_6$. Indeed, the yield strength (σ_y) and compressive strength (σ_f) values are found to be minimum for the Nb composition of 6 at.% ($NCSNb_6$) and the plastic strain (ε_p) value is also found to be maximum for the same. In general, during the blending of different elements with different atomic weights, there is every possibility for generating positive heating effect. This effect will create a heterogeneous atmosphere in the BMG matrix over the entire amorphous phase that can lead to the formation of a large number of shear bands across the whole volume, which results in an improvement of the plastic strain of BMG sample up to a certain extent [46, 47]. Also, the excess quantities of Niobium (Nb) doping of the base matrix may lead to the aggregation of Nb particles causing repulsive forces among the blended elements that may definitely hamper the plastic strain (ε_p) values of the BMG samples [47].

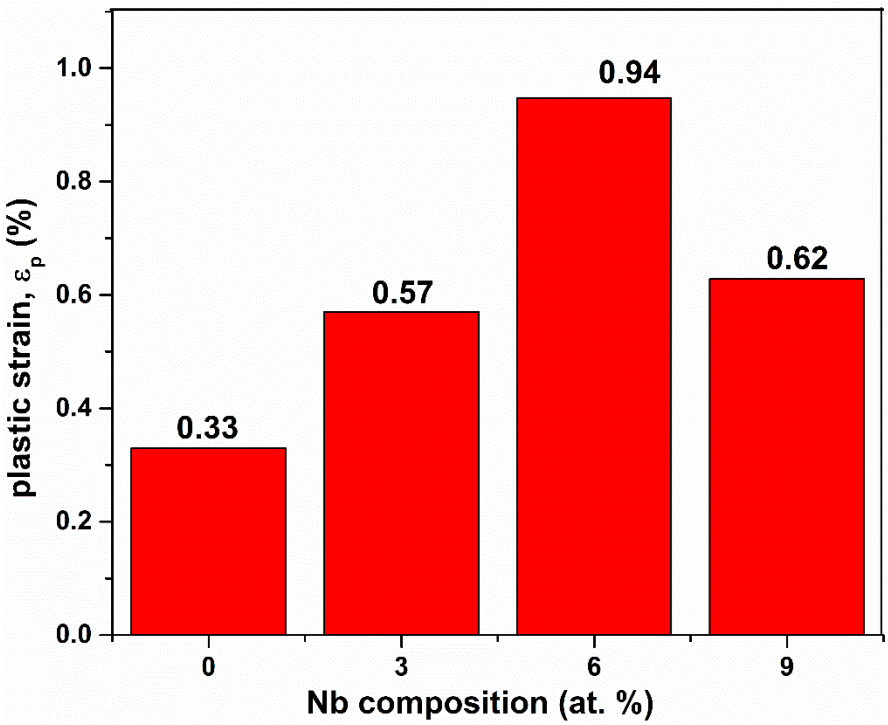

Figure 8. Compressive plasticity of all $NCSNb_x$ BMG samples

To further investigate the evidence of the deformation nature of as-prepared $NCSNb_x$ BMG samples, SEM analysis was done on these samples after the compression test and the results are displayed in Figure 9 (a-d). The images reveal that the homogeneity of the amorphous nature is retained even after 30 h of ball milling and the presence of Nb nano-crystallites can be seen in all the images as depicted in the TEM image of $NCSNb_6$ sample (Figure 3). From Figure 9 (a), a single-clustered morphology along with a considerable amount of porosity can be seen. However, this nature is gradually minimized with the doping of Niobium (Nb) content up to 6 at.% ($NCSNb_6$) (Figure 9 (c)). Moreover, uncontrolled aggregation of Nb nano-crystallites and cracks can be observed above 6 at.% (Figure 9 (d)). Therefore, it can be inferred that the structural morphology of $NCSNb_6$ can be the best plastic and also the best corrosive resistant sample when compared to the other BMGs under investigation.

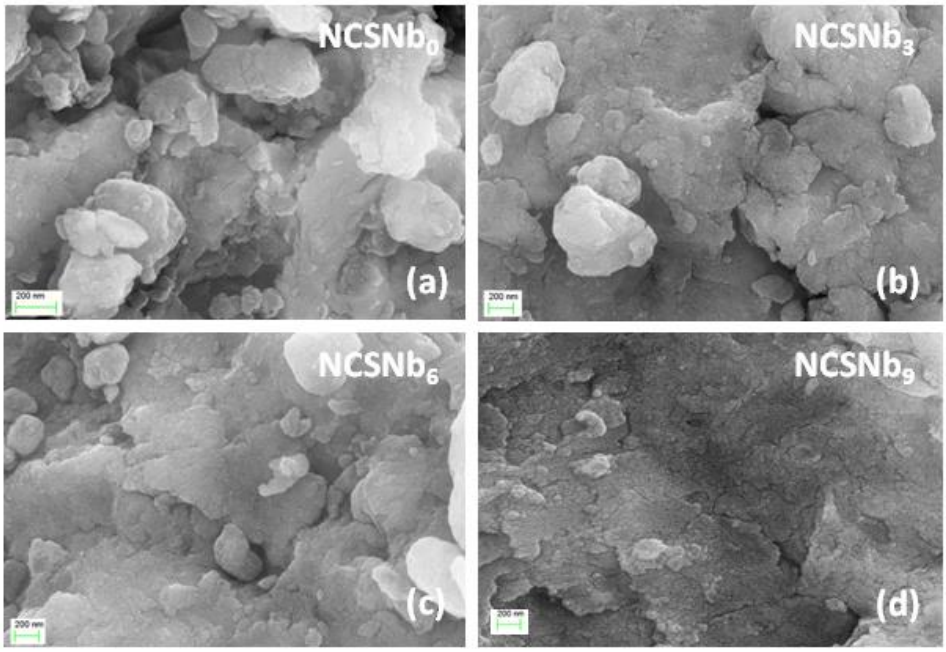

Figure 9. SEM Image Analysis of all $NCSNb_x$ BMG samples at 30 h of ball milling after compression tests: (a) A single-crystal morphology of Nb free BMG sample ($NCSNb_0$), (b) $NCSNb_3$ BMG sample, (c) $NCSNb_6$ BMG sample, and (d) $NCSNb_9$ BMG sample

Further, to study the corrosive properties of the as-prepared $NCSNb_x$ BMG samples, a potentio-dynamic polarization test was also performed from -2.5V~5.5V in 0.5 M HCl solution, with a potential sweep rate of 0.05mV/s. The anodic and cathodic polarization curves from Figures 10 (a) and (b), exhibit similar polarization tendency. From Figure 10 (a), it is noticed that the anodic curve does not hold good Tafel curve, which means that these curves for all the present BMG samples exhibit active or passive transition. However, their slopes can be extrapolated back to the open-circuit corrosion potential. From Figure 10 (b), the anodic current density (i_p) is calculated by summing the experimental anodic current density with extrapolated cathodic current density (i_c) (Table 4). It is noticed from Table 4 that the anodic current density (i_p) increases sharply before reaching a stable value, with a slight increase in the anodic polarization. This might

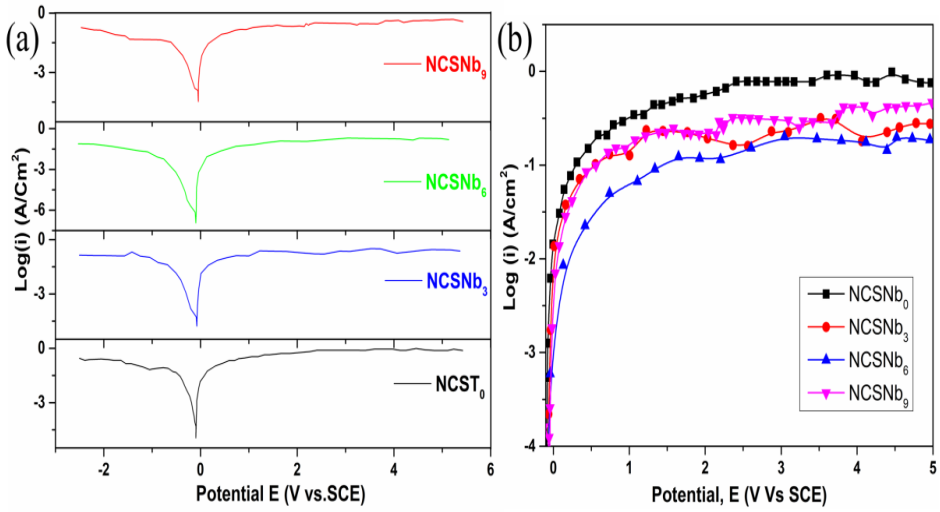

Figure 10. (a) Potentio-metric analysis of all $NCSNb_x$ samples at 30 h of ball milling-anodic current density with corrosion potential, (b) Potentio-metric analysis of $NCSNb_x$ BMG samples at 30 h of ball milling-magnification images of Figure 10 (a)

Table 4. Corrosion potential (E_c), passive potential (E_p), corrosion current density (i_c), and passive current density (i_p) of all $NCSNb_x$ BMG samples

BMG	E_c (mV)	E_p (V)	i_c (A/cm^2)	i_p (A/cm^2)
$NCSNb_0$	-107.1	1.2093	$3.8x10^{-2}$	0.5785
$NCSNb_3$	-80.2	0.7321	$1.7x10^{-2}$	0.7529
$NCSNb_6$	-65.4	0.5120	$5.2x10^{-3}$	0.0062
$NCSNb_9$	-94.7	1.1025	$4.1x10^{-2}$	0.4512

be due to the corrosion tendency of the BMG network. It is also known that for the best corrosive resistant sample, the corrosive current density should be smaller. The i_c ($5.2x10^{-3}$ A/cm^2) and i_p (0.0062 A/cm^2) values of the $NCSNB_6$ BMG sample are expected to be smaller when compared with the other prepared samples of BMGs under investigation which shows its active nature towards corrosion resistance. On the other hand, the step height and serration fluctuation and the corrosion potential value, E_c is highest for the best corrosion-resistant sample ($NCSNb_6$) (Figure 10 (b)). The results show that all the prepared samples of $NCSNb_x$ BMGs exhibit self-passivization behavior. Additionally, E_p value is found to increase at first until x = 6 at.%, indicating a chance of self-passivization and then decreases after x>6 at. %. As the i_p value of $NCSNb_6$ is of two orders of magnitude lesser than the other prepared samples of Ni-based BMGs, this would make it clear that the $NCSNb_6$ sample is comparatively less prone to passive film formation and is the best corrosion-resistant BMG sample. The compositional correlation curves of E_c Vs i_c and E_p Vs i_p are depicted in Figures 11 (a) and (b), respectively, show and prove the active nature of $NCSNb_6$ BMG sample towards corrosion resistance and self-passivization behaviour.

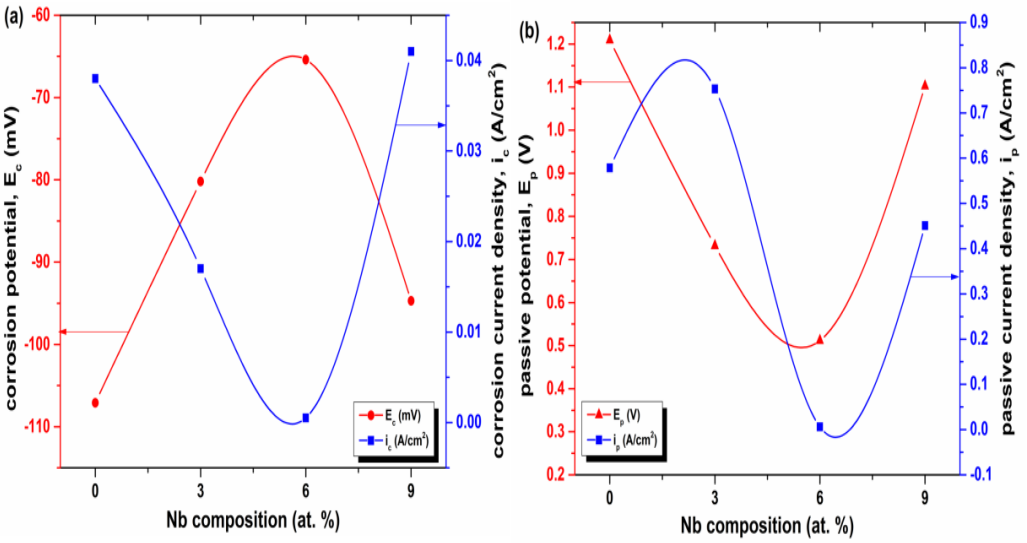

Figure 11. (a) Compositional dependence between corrosion current density (i_c) and corrosion potential (E_c) values of all $NCSNb_x$ BMG samples, (b) Compositional dependence between passive current density (i_p) and passive potential (E_p) values of all $NCSNb_x$ BMG samples

Lastly, to better understand the corrosion properties, the SEM morphologies of the prepared BMG samples after potentio-dynamic polarization tests are taken (Figure 12). It can be observed that Niobium free ($NCSNb_0$) BMG sample (Figure 12 (a)) is more prone to corrosion. It can be seen that sufficient doping of the base metal BMG matrix, with Niobium (Nb), definitely produces an improvement in the surface film structure (Figures 12 (b-d)). The images show the separation of passive films from the standard matrix, which may be caused by corrosion attack. Doping with Niobium (Nb) builds a protective surface film with more chemical stability and more corrosive resistance with a chloride medium. It is also clearly seen that the corroded surface of $NCSNb_6$ (Figure 12(c)) is more unstable and looser than the other BMGs.

The corrosion behavior of all the $NCSNb_x$ BMGs can be related to the variable content of alloying elements. For the prepared samples of BMGs, the atomic percentages of Nickel (Ni), Chromium (Cr) and Silicon (Si), decrease as x increases from 0 at.% to 9 at.%. But, the Niobium (Nb) atomic percentage increases with increasing x. A larger electrochemical potential discrepancy of the alloying elements allows the selective dissolution of Chromium (Cr) in [Ni-Cr-Si] BMG. With the increase of potential, the Chromium (Cr) found on the surface could be re-deposited into the pits, a process that accelerate pits propagation [48, 49]. Even though Ni can form oxides, Cr and Si are chemically more stable and structurally denser. A good corrosion-resistant BMG always has a dense uniform passive film that contains strong passive elements [50-52]. The i_p value indicates corrosion rate and E_c value indicates corrosion tendency. So, the higher corrosive resistance and low E_c and i_p of $NCSNb_6$ BMG sample would be a potential candidate for light-weight vehicle applications.

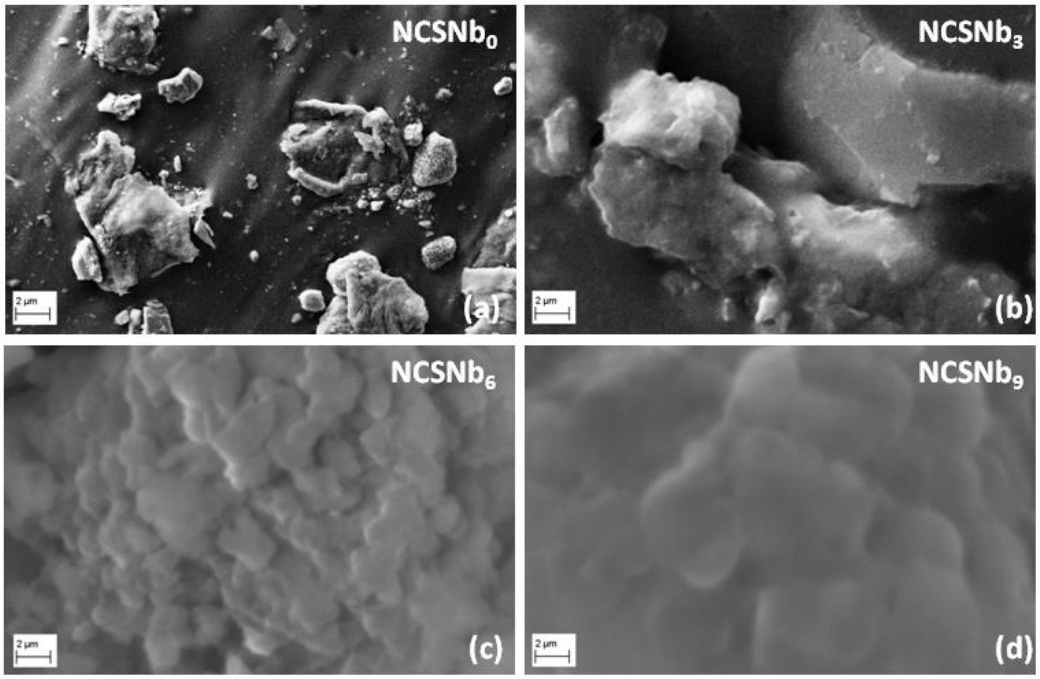

Figure 12. SEM micrographs of the corroded surfaces of all prepared $NCSNb_x$ BMG samples

4. Conclusions

The XRD results reveal that $NCSNb_6$ BMG contains more than 95% of the original compound and can be considered as the BMG with the best glass-forming ability (GFA). The greater the values of the super-cooled liquid region, ΔT and the GFA parameter, γ, the higher will be the glass-forming ability. So, the DTA reports are also in accordance with XRD results. The Vickers hardness test and the Uniaxial compression test confirm that all the prepared samples show work hardening behavior and is comparatively lesser for $NCSNb_6$ and also have high hardness value compared to all the other BMG samples. The σ_y (yield strength), σ_f (fracture strength) are respectively, in the range of 1.3-1.7 Gpa and 1.4-1.73 Gpa. The plastic strain value, ε_p of $NCSNb_6$ is the highest among all the studied $NCSNb_x$ BMG samples and reaches a maximum of 0.947±0.1%. Potentio-dynamic polarization tests also report lower values of i_p and i_c, further confirming that $NCSNb_6$ is the best corrosive resistant sample. The final SEM micrographs, after the corrosion test, show more unstable and looser patterns of the corroded surface of $NCSNb_6$, which further agrees with the results of potentio-dynamic test. This confirms that $NCSNb_6$ is the best corrosive resistant sample with good glass-forming abilities and mechanical strength.

5. Acknowledgements

The author wishes to thank Prof. Jonnalagadda B. Srikanth, School of Chemistry and Physics, University of KwaZulu Natal (UKZN), Westville Campus, Durban, South Africa for his kind support to carry out electron microscopy images and analysis.

References

[1] Klement, W., Willens, R.H. and Duwez, P.O.L., 1960. Non-crystalline structure in solidified gold-Silicon alloys. *Nature*, 187(4740), 869-870.

[2] Hofmann, D.C., 2013. Bulk metallic glasses and their composites: a brief history of diverging fields. *Journal of Materials*, 2013, https://doi.org/10.1155/2013/517904

[3] Chen, M. 2011. A brief overview of bulk metallic glasses: A review. *NPG Asia Materials*, 3, 82-90.

[4] Choi-Yim, H. and Johnson, W.L., 1997. Bulk metallic glass matrix composites. *Applied Physics Letters*, 71(26), 3808-3810.

[5] Inoue, A., 1998. Bulk Amorphous *Alloys: Preparation and Fundamental Characteristics*. Uetikon-Zürich: Trans Tech Publications.

[6] Inoue, A., 1999. *Bulk Amorphous Alloys: Practical Characteristics and Applications.* Vol. 6. Uetikon-Zürich: Trans Tech Publications.

[7] Suryanarayana, C. and Inoue, A., 2011. *Bulk Metallic Glasses*, 208-211. Boca Raton: CRC Press.

[8] Lu, Z.P. and Liu, C.T., 2004. Role of minor alloying additions in formation of bulk metallic glasses: A review. *Journal of Materials Science*, 39(12), 3965-3974.

[9] Peker, A. and Johnson, W.L., 1993. A highly processable metallic glass: $Zr_{41.2}Ti_{13.8}Cu_{12.5}Ni_{10.0}Be_{22.5}$. *Applied Physics Letters*, 63(17), 2342-2344.

[10] Park, E.S. and Kim, D.H., 2005. Design of bulk metallic glasses with high glass forming ability and enhancement of plasticity in metallic glass matrix composites: A review. *Metals and Materials International*, 11(1), 19-27.

[11] Feng, Y., Cai, A.H., Ding, D.W., Liu, Y., Wu, H., An, Q., Ning, H., Zhou, G.J. and Peng, Y.Y., 2019. Composition design and properties of Cu-Zr-Ti bulk metallic glass composites. *Materials Chemistry and Physics*, 232, 452-459.

[12] Wang, D., Li, Y., Sun, B.B., Sui, M.L., Lu, K. and Ma, E., 2004. Bulk metallic glass formation in the binary Cu-Zr system. *Applied Physics Letters*, 84(20), 4029-4031.

[13] Xia, L., Li, W.H., Fang, S.S., Wei, B.C. and Dong, Y.D., 2006. Binary Ni-Nb bulk metallic glasses. *Journal of Applied Physics*, 99, 026103-026106.

[14] Senkov, O.N. and Scott, J.M., 2005. Glass forming ability and thermal stability of ternary Ca-Mg-Zn bulk metallic glasses. *Journal of Non-crystalline Solids*, 351(37-39), 3087-3094.

[15] Schuster, B.E., Wei, Q., Hufnagel, T.C. and Ramesh, K.T., 2008. Size-independent strength and deformation mode in compression of a Pd-based metallic glass. *Acta Materialia*, 56(18), 5091-5100.

[16] Sun, Y.J., Qu, D.D., Huang, Y.J., Liss, K.D., Wei, X.S., Xing, D.W. and Shen, J., 2009. Zr-Cu-Ni-Al bulk metallic glasses with superhigh glass-forming ability. *Acta Materialia*, 57(4), 1290-1299.

[17] Liu, C.T. and Lu, Z.P., 2005. Effect of minor alloying additions on glass formation in bulk metallic glasses. *Intermetallics*, 13(3-4), 415-418.

[18] Kui, H.W., Greer, A.L. and Turnbull, D., 1984. Formation of bulk metallic glass by fluxing. *Applied Physics Letters*, 45(6), 615-616.

[19] Niu, H.Y., Cao, F.F., Deng, K.K., Nie, K.B., Kang, J.W. and Wang, H.W., 2020. Microstructure and corrosion behavior of the As-extruded Mg-4Zn-2Gd-0.5 Ca alloy. *Acta Metallurgica Sinica (English Letters)*, 33(3) 362-374.
[20] Warren, B.E., 1990. *X-ray Diffraction*. North Chelmsford: Courier Corporation.
[21] Egami, T., 2010. Understanding the properties and structure of metallic glasses at the atomic level. *Journal of Materials*, 62(2), 70-75.
[22] Wang, X.D., Bednarcik, J., Franz, H., Lou, H.B., He, Z.H., Cao, Q.P. and Jiang, J.Z., 2009. Local strain behavior of bulk metallic glasses under tension studied by in situ x-ray diffraction. *Applied Physics Letters*, 94(1), 011911-011913
[23] Stoica, M., Das, J., Bednarčik, J., Wang, G., Vaughan, G., Wang, W.H. and Eckert, J., 2010. Mechanical response of metallic glasses: Insights from in-situ high energy x-ray diffraction. *Journal of Materials*, 62(2), 76-82.
[24] Zhou, W., Zhang, C., Sheng, M. and Hou, J., 2016. Glass forming ability and corrosion resistance of Zr-Cu-Ni-Al-Ag bulk metallic glass. *Metals*, 6(10), 230- 236
[25] Lu, Z.P., Bei, H. and Liu, C.T., 2007. Recent progress in quantifying glass-forming ability of bulk metallic glasses. *Intermetallics*, 15(5-6), 618-624.
[26] Kivelson, D., Kivelsonb, S.A., Zhao, X., Nussinovb, Z. and Tarjusc, G., 1995. A thermodynamic theory of supercooled liquids. *Physica A: Statistical Mechanics and Its Applications*, 219(1), 27-38
[27] Debenedetti, P.G. and Stillinger, F.H., 2001. Supercooled liquids and the glass transition. *Nature*, 410(6825), 259-267.
[28] Li, Y.H., Zhang, W., Dong, C., Qiang, J.B., Xie, G.Q., Fujita, K. and Inoue, A., 2012. Glass-forming ability and corrosion resistance of Zr-based Zr-Ni-Al bulk metallic glasses. *Journal of Alloys and Compounds*, 536, S117-S121.
[29] Fathi, M., Safavi, M.S., Mirzazadeh, S., Ansariyan, A. and Ahadzadeh, I., 2020. A promising horizon in mechanical and corrosion properties improvement of Ni-Mo coatings through incorporation of Y_2O_3 nanoparticles. *Metallurgical and Materials Transactions A*, 51(2), 897-908.
[30] Maddin, R. and Masumoto, T., 1972. The deformation of amorphous palladium-20 at.% Silicon. *Materials Science and Engineering*, 9, 153-162.
[31] Argon, A.S., 1979. Plastic deformation in metallic glasses. *Acta Materilia.*, 27(1), 47-58.
[32] Hufnagel, T.C., Ott, R.T. and Almer, J., 2006. Structural aspects of elastic deformation of a metallic glass. *Physical Review B*, 73(6), 064204.
[33] Schuh, C.A., Hufnagel, T.C. and Ramamurty, U., 2007. Mechanical behavior of amorphous alloys. *Acta Materialia*, 55(12), 4067-4109.
[34] Tian, L., Cheng, Y.Q., Shan, Z.W., Li, J., Wang, C.C., Han, X.D., Sun, J. and Ma, E., 2012. Approaching the ideal elastic limit of metallic glasses. *Nature Communications*, 3(1), 1-6.
[35] Egami, T., Iwashita, T. and Dmowski, W., 2013. Mechanical properties of metallic glasses. *Metals*, 3(1), 77-113.
[36] Langer, J.S., 2008. Shear-transformation-zone theory of plastic deformation near the glass transition. *Physical Review E*, 77(2), 021502.
[37] Trexler, M.M., and Thadhani, N.N., 2010. Mechanical properties of bulk metallic glasses. *Progress in Materials Science*, 55(8), 759-839.
[38] Wang, S.L., Li, H.X., Zhang, X.F. and Yi, S., 2009. Effects of Cr contents in Fe based bulk metallic glasses on the glass forming ability and the corrosion resistance. *Materials Chemistry and Physics*, 113(2-3), 878-883.
[39] Chang, Z., Wang, W., Ge, Y., Zhou, J. and Cui, Z., 2018. Microstructure and mechanical properties of Ni-Cr-Si-B-Fe composite coating fabricated through laser additive manufacturing. *Journal of Alloys and Compounds*, 747, 401-407.

[40] Qiu, C.L., Liu, L., Sun, M. and Zhang, S.M., 2005. The effect of Nb addition on mechanical properties, corrosion behavior, and metal-ion release of ZrAlCuNi bulk metallic glasses in artificial body fluid. *Journal of Biomedical Materials Research Part A*, 75(4), 950-956.

[41] Pang, S.J., Zhang, T., Asami, K. and Inoue, A., 2002. Bulk glassy Fe-Cr-Mo-C-B alloys with high corrosion resistance. *Corrosion Science*, 44(8), 1847-1856.

[42] Naka, M., Hashimoto, K. and Masumoto, T., 1976. High corrosion resistance of Chromium-bearing amorphous iron alloys in neutral and acidic solutions containing chloride. *Corrosion*, 32(4), 146-152.

[43] Adylov, G.T., Voronov, V.G. and Sigalov, L.M., 1987. The system Nd_2O_3-Y_2O_3. *Inorganic Materials*, 23(11), 1644-1646.

[44] Shibli, S.M.A., Chinchu, K.S. and Sha, M.A., 2019. Development of nano-tetragonal Zirconia-Incorporated Ni-P coatings for high corrosion resistance. *Acta Metallurgica Sinica (English Letters)*, 32(4), 481-494.

[45] Lu, Z.P. and Liu, C.T., 2002. A new glass-forming ability criterion for bulk metallic glasses. *Acta Materialia*, 50(13), 3501-3512.

[46] Nieh, T.G., Yang, Y., Lu, J. and Liu, C.T., 2012. Effect of surface modifications on shear banding and plasticity in metallic glasses: An overview. *Progress in Natural Science: Materials International*, 22(5), 355-363.

[47] Park, E.S., Kim, D.H., Ohkubo, T. and Hono, K., 2005. Enhancement of glass forming ability and plasticity by addition of Nb in Cu-Ti-Zr-Ni-Si bulk metallic glasses. *Journal of Non-Crystalline Solids*, 351(14-15), 1232-1238.

[48] Pang, S.J., Zhang, T., Asami, K. and Inoue, A., 2002. Synthesis of Fe-Cr-Mo-C-B-P bulk metallic glasses with high corrosion resistance. *Acta Materialia*, 50(3), 489-497.

[49] Souza, C.A.C., Ribeiro, D.V. and Kiminami, C.S., 2016. Corrosion resistance of Fe-Cr-based amorphous alloys: An overview. *Journal of Non-Crystalline Solids*, 442, 56-66.

[50] Qin, C.L., Zhang, W., Asami, K., Kimura, H., Wang, X.M. and Inoue, A., 2006. A novel Cu-based BMG composite with high corrosion resistance and excellent mechanical properties. *Acta Materialia*, 54(14), 3713-3719.

[51] Asami, K., Qin, C.L., Zhang, T. and Inoue, A., 2004. Effect of additional elements on the corrosion behavior of a Cu-Zr-Ti bulk metallic glass. *Materials Science and Engineering: A*, 375, 235-239.

[52] Tang, J., Wang, Y., Zhu, Q., Chamas, M., Wang, H., Qiao, J., Zhu, Y. and Normand, B., 2018. Passivation behavior of a $Zr_{60}Cu_{20}Ni_8Al_7Hf_3Ti_2$ bulk metallic glass in sulfuric acid solutions. *International Journal of Electrochemical Science*, 13, 6913-6929.